Optical frequency measurements of $6s\,^2S_{1/2}-6p\,^2P_{3/2}$ transition in a ^{133}Cs atomic beam using a femtosecond laser frequency comb

V. Gerginov and C. E. Tanner*
Department of Physics, University of Notre Dame, Notre Dame, Indiana 46556-5670, USA

S. Diddams, A. Bartels, and L. Hollberg
Time and Frequency Division, National Institute of Standards and Technology, 325 Broadway M.S. 847, Boulder, Colorado 80305, USA
(Received 5 April 2004; published 20 October 2004)

Optical frequencies of the hyperfine components of the D_2 line in ^{133}Cs are determined using high-resolution spectroscopy and a femtosecond laser frequency comb. A narrow-linewidth probe laser excites the $6s\,^2S_{1/2}(F=3,4)\rightarrow 6p\,^2P_{3/2}(F=2,3,4,5)$ transition in a highly collimated atomic beam. Fluorescence spectra are taken by scanning the laser frequency over the excited-state hyperfine structure. The laser optical frequency is referenced to a Cs fountain clock via a reference laser and a femtosecond laser frequency comb. A retroreflected laser beam is used to estimate and minimize the Doppler shift due to misalignment between the probe laser and the atomic beam. We achieve an angular resolution on the order of 5×10^{-6} rad. The final uncertainties ($\sim\pm5$ kHz) in the frequencies of the optical transitions are a factor of 20 better than previous results [T. Udem *et al.*, Phys. Rev. A **62**, 031801 (2000).]. We find the centroid of the $6s\,^2S_{1/2}\rightarrow 6p\,^2P_{3/2}$ transition to be $f_{D2}=351\,725\,718.4744(51)$ MHz.

DOI: 10.1103/PhysRevA.70.042505 PACS number(s): 32.30.−r, 42.62.Fi, 06.30Ft, 42.60.Fc

I. INTRODUCTION

Precision measurement techniques in recent years have provided us with new ways to test fundamental theories in areas that lie outside of atomic physics. Tests of the standard model, a new value of the fine structure constant α, measurements of nuclear structure, and the weak interaction are possible using accumulated information about transition amplitudes and frequencies obtained through precision measurements [1–4]. Cesium, being one of the most thoroughly studied heavy atoms, is very suitable for these investigations, since the accuracy of atomic theory in this system is on the order of 1% [5]. In this respect, measurements of transition frequencies play a very important role, because the experimental accuracy can be many orders of magnitude better than accuracies obtained through atomic structure calculations. The results and level of accuracy obtained for the absolute transition frequencies presented here are of particular relevance to the interpretation of atom interferometry experiments involving cesium where the recoil energy and momentum transfer of single-photon interactions is required. Examples of new physics expected from combining absolute transition frequencies with atom interferometry include measurements of local gravity [6] and a new value for the fine structure constant [7].

A variety of techniques have been implemented to eliminate Doppler effects in optical frequency measurements of atomic transitions. These include saturated absorption spectroscopy in vapor cells [8,9], magneto-optic traps [10], and thermal atomic beams [11,12]. While vapor cell experiments are easier to implement, systematic effects due to optical pumping, magnetic fields, and light pressure limit the final uncertainty. In previous measurements of the $6s\,^2S_{1/2}\rightarrow 6p\,^2P_{3/2}$ transition in ^{133}Cs, the final uncertainty was limited by such systematic effects and not by optical frequency measurement techniques [8]. In atomic beams, Doppler broadening can be reduced geometrically to less than the natural linewidth for allowed transitions where it no longer imposes a limitation on determining the spectral line centers. In addition, optical pumping can be suppressed by working at low light intensity. With atomic beams, the most serious experimental problem is Doppler shifting of the resonances due to misalignment of the atomic beam with respect to the laser propagation direction. This problem is avoided with magneto-optic traps at the expense of a much more complicated system. In this work, we show that the Doppler shift caused by atomic and laser beam misalignment can be reduced to the level of other uncertainties with a simple experimental procedure.

II. EXPERIMENTAL SETUP

The experimental setup is shown in Fig. 1. The frequency detuning of a highly monochromatic probe laser with respect to a stable reference laser is measured by detecting a heterodyne beat note between the two lasers. The optical frequency of the reference laser is determined by measuring the beat note with a tooth of a self-referenced femtosecond laser frequency comb [13–15]. Using established techniques [16,17], the frequency comb is referenced to a stable hydrogen maser that has its frequency calibrated by a cesium atomic fountain clock [18]. The fractional frequency instability of the comb teeth is equivalent to that of the hydrogen maser, given by $\sim2\times10^{-13}\tau^{-1/2}$, with τ the integration time measured in seconds. When averaged for several hours, the frequency of each tooth of the femtosecond comb can be known relative to the cesium primary frequency standard with fractional uncertainty approaching a few parts in 10^{15}. In this way, the optical frequency of the probe laser can be determined using

*Electronic address: Carol.E.Tanner.1@nd.edu

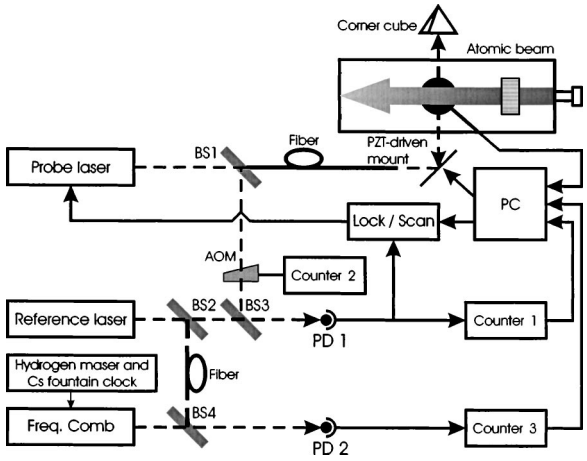

FIG. 1. Experimental setup.

the two beat-note measurements (probe laser with reference laser and reference laser with the comb). The spectroscopy is realized with the help of a highly collimated thermal atomic beam apparatus. Part of the probe laser output is sent through a single-mode fiber to the vacuum chamber and excites the atomic beam at a right angle. The deviation of this angle from 90° is determined and corrected during the measurement process to better than 5×10^{-6} rad. The fluorescence from the excited atoms is measured together with the probe laser optical frequency, and analyzed using a FORTRAN program.

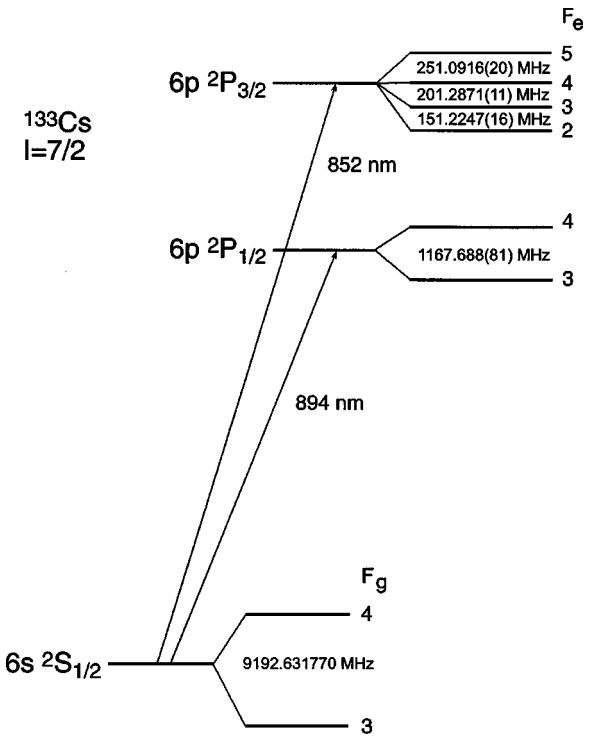

FIG. 2. ^{133}Cs energy level diagram.

Helmholtz coils and is measured to be less than 2×10^{-6} T with a commercial magnetometer.

A. Atomic beam

The lowest-lying energy levels of ^{133}Cs are shown in Fig. 2. The thermal beam apparatus is described in detail in [19]. A rectangular profile (13 mm$\times$15 mm) atomic beam with a density on the order of 3×10^{13} cm^{-3} is created in a vacuum chamber with a Cs reservoir, oven, and nozzle. The vacuum is better than 1.33×10^{-4} Pa. Due to the high density of the atomic beam, a liquid nitrogen trap is used to prevent the formation of any significant Cs thermal background. The atomic beam divergence is reduced to $\sim$12 mrad with a collimator, constructed from microscope cover slips, placed 12 cm away from the nozzle. The atomic beam passes above a large-area photodetector. A single-mode optical fiber is used to send part of the probe laser beam to the vacuum chamber. The laser beam polarization is aligned with the direction of the atomic beam propagation using a linear polarizer with an extinction ratio of 1/1000. The rectangular laser beam (7×7 mm^2, determined by the aperture of the polarizer) excites the atomic beam above the photodetector. Fluorescence from the excited atoms is focused on the photodetector by a curved mirror placed above the interaction region. A transimpedance amplifier with high gain is used to convert the photocurrent into voltage. An analog-to-digital board measures the voltage which is then recorded with a computer. The laser beam direction can be steered with a mirror on a piezoelectric-transducer (PZT) driven mount which is controlled by the computer. The magnetic field in the interaction region is compensated using three pairs of

B. Laser system and optical frequency measurements

The heterodyning laser system is described in detail in Ref. [20]. We use two spectrally narrowed 852-nm diode lasers. Their frequency difference is offset-locked to a computer-controlled rf synthesizer. The reference laser frequency is stabilized to a saturated absorption signal detected in a Cs vapor cell kept near room temperature. The probe laser is offset-locked to the reference laser and is scanned by changing the frequency of the rf synthesizer. The approximate frequency of the probe laser is determined by the rf lock and the computer, respectively. The beat note between the reference and probe laser is measured using the rf counter 1. The probe laser frequency is offset with an acousto-optic modulator (AOM) before the beat note with the reference laser is detected. This is done to avoid a zero beat note frequency when the probe laser is scanned in the vicinity of the Cs transitions that are used to lock the reference laser (either the $F_g=3\rightarrow F_e=2$ or $F_g=4\rightarrow F_e=5$ cycling transitions). This also reduces the technical noise in the measurement which is higher at low frequencies. The AOM frequency offset is measured using rf counter 2. The optical frequency of the reference laser is determined using the high-repetition-rate "self-referenced" femtosecond laser frequency comb, as described above. The rf counter 3 measures the beat note between the reference laser and one tooth of the frequency comb. The precision of counters 1 and 3 is set to six digits, or 1 kHz, and the precision of counter 2 is set to seven digits, or 0.1 kHz. A detailed description of the spectrum measure-

ment is given in [19]. The data acquisition system measures the fluorescence signal at a rate of 2000 samples per second for 0.5 s. The counters perform frequency measurements during the fluorescence data acquisition. To calibrate the frequencies and determine the laser instabilities for each data point, counters 1 and 3 measure the beat note and perform statistics of four frequency measurements and counter 2 measures the AOM frequency offset by performing a single frequency measurement. After the measurements are done, the computer collects the data from the counters, averages the fluorescence signal, and stores the mean value and the standard deviation of the fluorescence signal and the frequency measurements. Measuring the optical frequency of the reference laser, the beat note between the reference and probe lasers, and the probe laser frequency offset, we determine the optical frequency of the probe laser to better than 10 kHz during each time interval of 0.5 s. The uncertainty in the frequency calibration is due to the jitter of the reference diode laser frequency caused by mechanical instabilities of its external cavity [20]. After each measurement the computer changes the frequency of the rf synthesizer, thus scanning the probe laser frequency to a new value. The frequency of the probe laser is scanned over a range greater than 550 MHz to record the complete excited-state hyperfine structure.

C. Theoretical model

It is very important to understand the details of the line shapes of the components in the measured spectra. When the probe laser beam and the atomic beam are exactly perpendicular, the frequency dependence of the excited-state fluorescence is described by a Voigt profile [19]. We assume that the optical frequencies of the different M_{F_g}, M_{F_e} Zeeman components belonging to the same ground (F_g) or excited (F_e) state component are equal because of the static magnetic field compensation. This means that for each transition component $6s\,^2S_{1/2}(F_g) \rightarrow 6p\,^2P_{3/2}(F_e)$ there is a single Voigt profile to calculate. In our fitting program (using the Levenberg-Marquardt minimization method taken from [21]), the Doppler width of the Voigt profiles is constrained to be the same for all spectral components. The Lorentzian parts of the individual Voigt profiles are fit independently. Due to possible formation of a Cs cloud inside the chamber, the model function also includes a Gaussian profile for each spectral component with a full width at half maximum (FWHM) determined by the oven temperature of 443 K. For each component of the spectrum, the Gaussian background amplitude is proportional to the corresponding Voigt profile amplitude with a fitting parameter which is the same for all components in the spectrum. The model includes a dc offset as a parameter to account for the photodetector leakage current and scattered laser light hitting the photodetector. A linear slope parameter is used to account for possible changes in the scattered laser light.

III. MEASUREMENT PROTOCOL

When the probe laser beam is not exactly perpendicular to the atomic beam direction, the optical frequencies of the transitions of interest will be Doppler shifted, and the resulting line shapes are no longer symmetric [19]. This produces two types of systematic effects: one due to the Doppler shift itself and the other due to the inaccurate fit which assumes symmetric line shapes. To measure and minimize these two effects, a corner cube is used to retroreflect the incident laser beam back into the interaction region. The Doppler shift of the spectrum created by the counterpropagating laser beam has an opposite sign to that of the initial laser beam. The intensity of the counterpropagating beam is 70% of the incident beam intensity (both of which are well below the saturation intensity), due to reflection losses from the vacuum system output window and the corner cube. Fluorescence from both beams is generated in the same spatial region and is detected by the large-area photodetector. For a specific angle between the atomic and laser beams, spectra are recorded for the two configurations—with and without a counterpropagating laser beam. The two types of spectra are then fitted with the model described in the previous section. Several data files for the same configuration are fitted, giving a mean value and a standard deviation for the optical frequency of each transition component. We take the standard deviation as a measure of the uncertainty in the mean. Usually, four files are enough to give a standard deviation of the fit of <5 kHz. When fitted, the peaks in the two-beam spectra have frequency centers slightly different from those of the incident beam alone. This difference is a measure of the deviation of the laser incidence angle from 90°. We minimize this deviation by changing the laser beam incidence angle, steering the mirror that is mounted on the computer-controlled PZT-driven mount. This mount has a measured angular resolution corresponding to a Doppler shift of 365 Hz per step.

A. Measurements from the $F_g=3$ ground-state component

The reference laser is locked to the $6s\,^2S_{1/2}(F_g=3) \rightarrow 6p\,^2P_{3/2}(F_e=2)$ cycling transition. The part of the probe laser beam used in the frequency measurement has its optical frequency shifted up by 85 MHz using an AOM. The cesium oven is kept at $T=443$ K and the Cs reservoir at $T=393$ K. The typical laser intensity is $I=2\ \mu\mathrm{W/cm^2}$, approximately 1/500 of the saturation intensity of the strongest line component $(F_g=4 \rightarrow F_e=5)$. The reference laser frequency is $\sim$10 MHz higher than the optical frequency f_n of one tooth of the femtosecond laser frequency comb. A typical one-beam spectrum is shown in Fig. 3.

B. Measurements from the $F_g=4$ ground-state component

In this case the reference laser is locked to the $6s\,^2S_{1/2}(F_g=4) \rightarrow 6p\,^2P_{3/2}(F_e=5)$ cycling transition. The part of the probe laser beam used in the frequency measurement has its optical frequency shifted down by 68 MHz using an AOM. The cesium oven is kept at $T=443$ K and the Cs reservoir at $T=393$ K. The typical laser intensity is $I=1\ \mu\mathrm{W/cm^2}$, approximately 1/1000 of the saturation intensity of the strongest line component $(F_g=4 \rightarrow F_e=5)$. The reference laser frequency is $\sim$10 MHz higher than the opti-

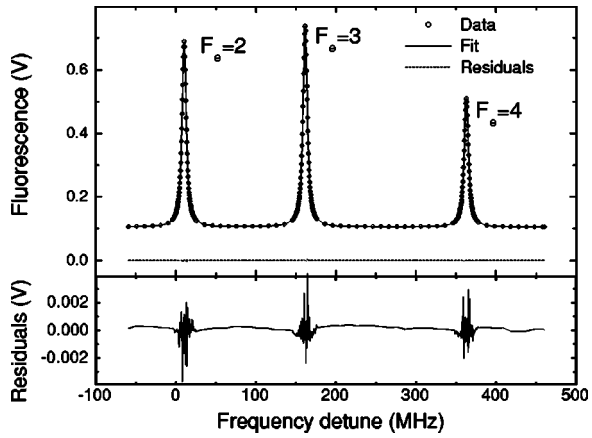

FIG. 3. Spectrum of the $6s\,^2S_{1/2} \rightarrow 6p\,^2P_{3/2}$ transition in ^{133}Cs taken with the probe laser exciting $F_g=3$ ground-state component. The optical frequency f_n of the femtosecond laser tooth has been subtracted from the data. The top graph shows experimental points, theoretical fit, and residuals (dotted line) on the same scale. The bottom graph shows the residuals on a different scale.

cal frequency f_n of a different tooth of the femtosecond laser frequency comb. A typical one-beam spectrum is shown in Fig. 4.

IV. RESULTS AND DISCUSSION

For each angle between the laser and atomic beam, the mean value and the standard deviation for the optical frequencies of each transition are compared for the one- and two-beam configurations, and the difference is minimized by changing the angle between the laser and the atomic beam. The values of the optical frequencies for which the difference is less than 5 kHz are used to find the optical frequency of each spectral component. The uncertainty evaluation is explained in the next section. The data for one- and two-beam spectra are shown in Figs. 5 and 6. The weighted mean values of the optical frequencies between the ground- and excited-state components have been subtracted from the data. The weighted mean has been corrected for the frequency shifts that arise from optical pumping and recoil effects with the estimated values listed in Table I, as is described in the following section. The weighted mean values with their uncertainties are listed in Table II.

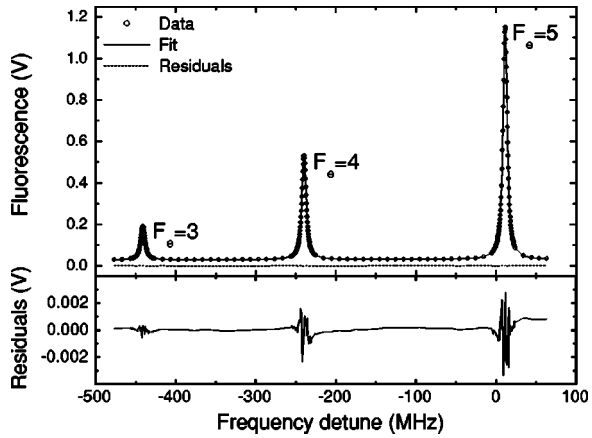

FIG. 4. Spectrum of the $6s\,^2S_{1/2} \rightarrow 6p\,^2P_{3/2}$ transition in ^{133}Cs taken with the probe laser exciting $F_g=4$ ground-state component. The optical frequency f_n of the femtosecond laser tooth has been subtracted from the data. The top graph shows experimental points, theoretical fit, and residuals (dotted line) on the same scale. The bottom graph shows the residuals on a different scale.

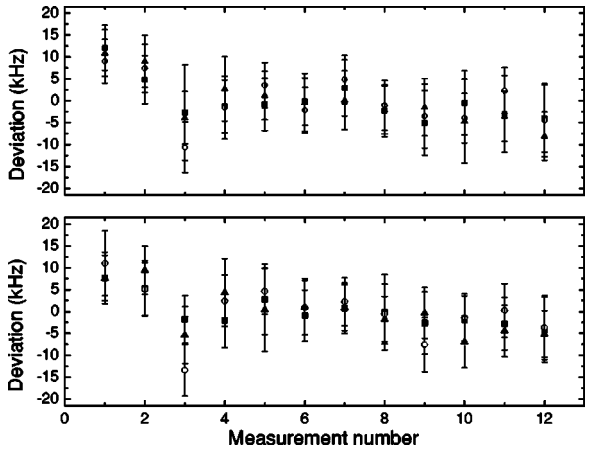

FIG. 5. Difference from the mean of measured optical frequencies between the $6s\,^2S_{1/2}(F_g=3)$ ground state and the three excited-state hyperfine components $6p\,^2P_{3/2}$ ($F_e=2$, squares; $F_e=3$, open circles; $F_e=4$, triangles). Upper trace, one-beam data; lower trace, two-beam data. The data were taken on different days over a month period. Each point represents the average of four scans.

A. Error budget

We determine the final values of the optical frequencies and their uncertainties as described in this section. The center of each line and its statistical uncertainty is determined by fitting several data files, as explained in Sec. III. To these

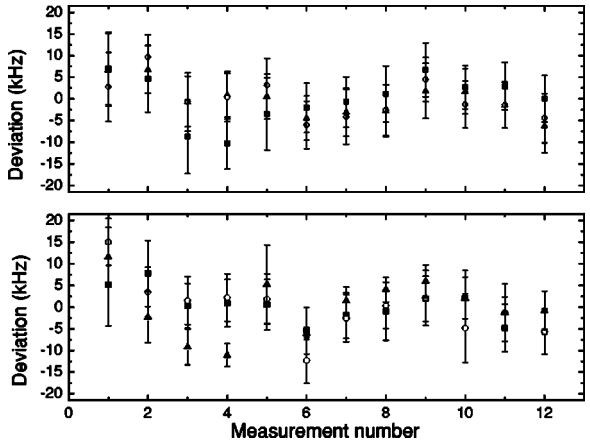

FIG. 6. Difference from the mean of measured optical frequencies between the $6s\,^2S_{1/2}(F_g=4)$ ground state and the three excited-state hyperfine components $6p\,^2P_{3/2}$ ($F_e=3$, squares; $F_e=4$, open circles; $F_e=5$, triangles). Upper trace, one-beam data; lower trace, two-beam data. The data were taken on different days over a month period. Each point represents the average of four scans.

TABLE I. Statistical and systematic uncertainties in kHz. For the intensity dependent shift (rows 3 and 4), we show the correction that has to be made to the optical frequency values when extrapolating to zero laser intensity. The uncertainty associated with this correction is given in brackets.

	$3\rightarrow2$	$3\rightarrow3$	$3\rightarrow4$	$4\rightarrow3$	$4\rightarrow4$	$4\rightarrow5$
Statistical (fit+Doppler)[a]	±1.9	±1.7	±1.8	±1.8	±1.6	±1.7
Statistical (fit+Doppler)[b]	±1.8	±1.7	±1.7	±1.7	±1.7	±1.7
Intensity dependent shift[a]	0.3(1.0)	3.3(1.0)	2.5(1.4)	−1.2(1.1)	−3.8(1.2)	−0.8(1.1)
Intensity dependent shift[b]	−2.1(1.3)	0.4(1.0)	1.1(1.0)	−1.1(1.3)	−1.4(1.8)	−0.6(1.8)
Corner cube	±5.0	±5.0	±5.0	±5.0	±5.0	±5.0
Zeeman effect	±1.0	±1.0	±1.0	±1.0	±1.0	±1.0
ac Stark shift	<0.1	<0.1	<0.1	<0.1	<0.1	<0.1

[a]One-beam data.
[b]Two-beam data.

uncertainties we add in quadrature the statistical uncertainty in minimizing the Doppler shift, estimated to be 5 kHz, to give a total statistical uncertainty. All fitted line centers with their total statistical uncertainties are shown in Figs. 5 and 6. These values are used to determine a weighted mean and an error in the weighted mean for one- and two-beam optical frequencies. We measure laser-intensity-dependent shifts that depend on the initial and final states studied and range from −3.8 kHz to 3.3 kHz. The frequency for each pair of states is obtained by extrapolating the mean values to zero laser intensity. We add in quadrature all evaluated systematic uncertainties to the error in the weighted mean for each frequency value. The final values and their uncertainties are given in rows 2, 3, 5, and 6 of Table II. In rows 1 and 4 of Table II are given the weighted average between one- and two-beam data where systematic uncertainties that are common to both types of data are added in quadrature after averaging. A discussion of each evaluated systematic effect appears below.

Systematic shifts and uncertainties have been evaluated for optical pumping, corner cube imperfections, recoil shift, the Zeeman effect, and the ac Stark effect. Optical pumping redistributes the initial level populations after the atoms have decayed to the ground state. In the presence of a residual magnetic field, this can lead to line shape asymmetries and to a systematic error. To minimize the effect, we reduce the magnetic field in the interaction region to less than 2×10^{-6} T, use linear laser polarization, and work at laser intensities on the order of 1/1000 of the saturation intensity. Residual shifts due to the optical pumping are determined by measuring the transition frequencies at different laser intensities and extrapolating their values to zero laser intensity. These shifts are taken into account in the final optical frequency values. The corner cube deviation from the right angle is given by the manufacturer to be less than 9.7×10^{-6} rad (2 arcsec), which gives a possible systematic effect on the order of ±5 kHz.

The peak of the single-photon absorption probability of an atom initially at rest is shifted from the energy difference between the atomic levels by the recoil energy given by $h\nu_r=h^2\nu_0^2/2M_{\mathrm{Cs}}c^2\approx2.1\ \mathrm{kHz}\times h$, where h is Planck's constant, $h\nu_0$ is the energy difference between atomic states, M_{Cs} is the mass of a Cs atom, and c is the speed of light. This recoil energy shift is independent of photon direction and is present in both one- and two-beam data. After the excited atoms have decayed back to the ground state, their average velocity change in the direction of the laser beam is one recoil velocity given by $V_r=h(\nu_0+\nu_r)/M_{\mathrm{Cs}}c\approx3.5\times10^{-3}$ m/s. Some fraction of the atoms may absorb more than one photon as they pass through the laser beam. These

TABLE II. Optical frequencies between different components of the $6s\,^2S_{1/2}\rightarrow6p\,^2S_{3/2}$ transition, measured in MHz. The one-beam and two-beam data are given. Rows 1 and 4 represent the averaged values between one- and two-beam data. The uncertainties in the values are explained in detail in Table I. For the averaged values in rows 1 and 4, the corner cube uncertainty of 5 kHz was added after the values in rows 2 and 3 (5 and 6, respectively) were averaged.

	$F_e=2$	$F_e=3$	$F_e=4$	$F_e=5$
$F_g=3$	351 730 549.6215(55)	351 730 700.8459(55)	351 730 902.1332(56)	
$F_g=3$[a]	351 730 549.6199(55)	351 730 700.8448(55)	351 730 902.1341(56)	
$F_g=3$[b]	351 730 549.6246(56)	351 730 700.8462(55)	351 730 902.1327(55)	
$F_g=4$		351 721 508.2105(55)	351 721 709.4969(55)	351 721 960.5857(55)
$F_g=4$[a]		351 721 508.2107(55)	351 721 709.4968(55)	351 721 960.5870(55)
$F_g=4$[b]		351 721 508.2102(55)	351 721 709.4971(57)	351 721 960.5838(57)

[a]One-beam data.
[b]Two-beam data.

atoms will have their velocity distribution shifted by one unit of recoil velocity for each additional photon depending on direction. This effect can cause asymmetries and shifts in the fluorescence line shape that can be minimized by keeping the intensity low and then extrapolating to zero. However, the intensity dependence of the velocity recoil effect cannot be easily separated from optical pumping without knowing the exact residual magnetic field present. From the ratio of the amplitudes between the cycling and open transitions and simple excitation probability calculations, we find that, on average, each atom scatters <1.2 photons at a laser intensity of 1 μW/cm^2 ($F_g=4$) or 2 μW/cm^2 ($F_g=3$). There is excellent agreement between the theoretical peak height ratios and the experimentally measured ratios (on the order of 3%, as shown in [3]), which confirms also that we work at laser intensities that cause no significant optical pumping. Given in rows 3 and 4 of Table I are the shifts required to extrapolate each optical transition frequency from its value at 1 μW/cm^2 for $F_g=4$ (2 μW/cm^2 for $F_g=3$) to zero intensity. Although it cannot be completely eliminated due to the 30% imbalance in the two laser beams, one would expect the portion of the intensity-dependent shift due to the recoil velocity to be reduced in the two-beam data compared to the one-beam data and this trend is exhibited by the shifts given in Table I.

The Zeeman effect could produce significant systematic effects in the optical frequency determination because of a deviation of the line shape from a Voigt profile when the different sublevels of the ground and excited states are no longer degenerate. This will also cause frequency shifts if optical pumping is present. We estimate the systematic uncertainty due to the Zeeman effect by applying a constant magnetic field of 1×10^{-4} T in the x, y, and z directions, respectively, and measure the changes in the optical frequency values. It is found that such a magnetic field, while producing a significant deviation between the data and the model, changes the values of the optical frequencies by less than 20 kHz. With the magnetic field compensated in the interaction region to better than 2×10^{-6} T, we place a conservative upper limit of 1 kHz on this systematic uncertainty. The ac Stark shift has been estimated previously [4] to be insignificant at these laser intensity levels.

The error budget for each optical transition is given in Table I where rows 1 and 2 give the error in the weighted mean for one- and two-beam data, respectively. Extrapolating to zero intensity requires adding to the results obtained at 1 μW/cm^2 ($F_g=4$) or 2 μW/cm^2 ($F_g=3$) the signed shifts that are given in rows 3 and 4 along with their uncertainties. The uncertainty in each shift is added in quadrature with the error in the weighted mean and the systematic uncertainties that appear in rows 5, 6, and 7. The extrapolated frequencies for both one- and two-beam data and their final uncertainties are given in rows 2, 3, 4, and 5 of Table II. The weighted averages of one- and two-beam data appear in rows 1 and 4 of Table II where the uncertainty due to corner cube imperfection is added in quadrature with the weighted uncertainties after the averaging. Rows 1 and 4 of Table II give our final optical frequency values with uncertainties for the six hyperfine components of this transition. These values correspond to the photon frequencies at which the maximum probability for single-photon absorption occurs and are expected to be the results most useful for the interpretation of atom interferometry experiments.

TABLE III. Excited-state hyperfine structure splittings, measured in MHz.

	$2\rightarrow3$	$3\rightarrow4$	$4\rightarrow5$
From [3]	151.2247(16)	201.2871(11)	251.0916(20)
From $F=3$[a]	151.2249(25)	201.2893(24)	
From $F=3$[b]	151.2217(25)	201.2865(24)	
From $F=4$[a]		201.2861(24)	251.0902(23)
From $F=4$[b]		201.2869(24)	251.0867(24)

[a]One-beam data.
[b]Two-beam data.

B. Results and comparison

Optical transitions to the $F_e=3$ and $F_e=4$ excited-state components can be made from both ground states. The difference between the optical frequencies of the transition components $6s\,^2S_{1/2}(F_g=3)\rightarrow6p\,^2P_{3/2}(F_e=3)$ and $6s\,^2S_{1/2}(F_g=4)\rightarrow6p\,^2P_{3/2}(F_e=3)$ must be equal to the ground-state hyperfine splitting f_{HFS}, which is an exact number and is used as the definition of the second. The same is true for the difference between the optical frequencies of the transition components $6s\,^2S_{1/2}(F_g=3)\rightarrow6p\,^2P_{3/2}(F_e=4)$ and $6s\,^2S_{1/2}(F_g=4)\rightarrow6p\,^2P_{3/2}(F_e=4)$. Using the optical frequencies for the one- and two-beam data, respectively, we find

$$f_{33}-f_{43}-f_{HFS}=2.3(4.4)\text{ kHz (one beam)}\quad\text{and }4.2(3.1)\text{ kHz (two beam)},$$

$$f_{34}-f_{44}-f_{HFS}=5.6(3.9)\text{ kHz (one beam)}\quad\text{and }3.8(3.5)\text{ kHz (two beam)}.$$

These uncertainties do not include the systematic uncertainty associated with the corner cube (5 kHz, row 5 in Table I) since it is the same for all optical transitions and will not affect the differences. The uncertainties are quadrature sums of uncertainties (rows 1, 2, 3, 4, and 6 in Table I) for both compared optical frequencies. Our data agree on the 1.5σ level which indicates no significant underestimation of our uncertainties. Another possible check is verifying the hyperfine splittings of the excited state which are known with a precision better than 2 kHz [3]. The excited-state hyperfine splittings are obtained by subtracting the corresponding optical frequencies, given in Table II. The values are given in Table III. The data agree with the previous results on the level of 1.5σ.

The optical frequencies of the different components of the ground $6s\,^2S_{1/2}$ and excited $6p\,^2P_{3/2}$ state have been previously measured with a quoted uncertainty of 110 kHz [8]. We find general agreement between the previous and our measurements except for the $F_g=4\rightarrow F_e=5$ transition where a deviation of 225 kHz exists, which is twice the experimental uncertainty reported in [8]. Since the $F_g=4\rightarrow F_e=5$ is the strongest component of the D_2 line, systematic effects arising from optical pumping and light pressure are expected to play significant role in this case in vapor cell saturated absorption experiments.

The optical frequencies given in Table II represent the photon frequencies at which the maximum probability for single-photon absorption occurs for each pair of states. Embedded in these values is the recoil energy shift $h\nu_r = h^2\nu_0^2/2M_{\mathrm{Cs}}c^2$ of the peak center relative to the energy difference between atomic levels. The energy centroid of the $6p\,^2P_{3/2}$ state relative to the energy centroid of the $6s\,^2S_{1/2}$ ground state is the energy difference in the absence of hyperfine structure and the recoil energy shift. Therefore, we express the frequency centroid of the $6s\,^2S_{1/2}$ to $6p\,^2P_{3/2}$ transition as

$$f_{D2} = \begin{cases} -\frac{21}{4}a - \frac{1}{4}b - c + \frac{7}{4}a_{6s_{1/2}} + f_{45} - \nu_r: & F_g = 4 \rightarrow F_e = 5, \\ -\frac{1}{4}a + \frac{13}{28}b + \frac{33}{7}c + \frac{7}{4}a_{6s_{1/2}} + f_{44} - \nu_r: & F_g = 4 \rightarrow F_e = 4, \\ \frac{15}{4}a + \frac{5}{28}b - \frac{55}{7}c + \frac{7}{4}a_{6s_{1/2}} + f_{43} - \nu_r: & F_g = 4 \rightarrow F_e = 3, \\ -\frac{1}{4}a + \frac{13}{28}b + \frac{33}{7}c - \frac{9}{4}a_{6s_{1/2}} + f_{34} - \nu_r: & F_g = 3 \rightarrow F_e = 4, \\ \frac{15}{4}a + \frac{5}{28}b - \frac{55}{7}c - \frac{9}{4}a_{6s_{1/2}} + f_{33} - \nu_r: & F_g = 3 \rightarrow F_e = 3, \\ \frac{27}{4}a - \frac{15}{28}b + \frac{33}{7}c - \frac{9}{4}a_{6s_{1/2}} + f_{32} - \nu_r: & F_g = 3 \rightarrow F_e = 2, \end{cases}$$

where f_{D2} is the frequency of the line centroid, a, b, and c are the excited-state hyperfine coupling constants [3], f_{FgFe} is the optical frequency between F_g ground- and F_e excited-state components, $a_{6s_{1/2}}=f_{HFS}/4$ is the ground-state hyperfine coupling constant, and ν_r is the recoil energy shift divided by Planck's constant h. At our present level of uncertainty, higher-order hyperfine contributions are negligible as we show in Ref. [3]. The value of $a_{6s_{1/2}}$ can be calculated from the ground-state splitting $f_{HFS}=9192.631\,770$ MHz. Using these expressions and statistically averaging all six measured frequencies, we determine the line centroid to be $f_{D2}=351\,725\,718.4744(51)$ MHz. Our result is in very good agreement with the value $f_{D2}=351\,725\,718.50(11)$ MHz of Udem *et al.* [8] but with significantly reduced uncertainty. Our uncertainty is similar to that obtained for the $5s\,^2S_{1/2}\rightarrow 5p\,^2P_{3/2}$ line in ^{87}Rb by Ye *et al.* [9].

V. CONCLUSIONS

We have measured the absolute optical frequencies of the six hyperfine components of the $6s\,^2S_{1/2}\rightarrow 6p\,^2P_{3/2}$ transition in ^{133}Cs with an accuracy of better than 2×10^{-11} and about 1/1000 of the natural linewidth of the transition. Our uncertainities represent a factor of 20 improvement over previous results [8]. All of our measured values agree with previous results except for the strongest hyperfine component, $F_g=4\rightarrow F_e=5$, where we find a discrepancy of 225 kHz which is about twice the previously quoted experimental uncertainty and about 1 part per billion of the optical frequency. Since atom interferometry experiments involving cesium are expected to reach precisions of order 1 part per billion and below [22,23], it is important that the work presented here eliminates this discrepancy.

ACKNOWLEDGMENTS

We would like to thank Sebastien Bize and Jim Bergquist for the helpful discussions and Feng-Lei Hong for his assistance with the femtosecond comb system. We would also like to thank Keith Calkins for thoroughly reading the manuscript. This project is supported by the Division of Chemical Sciences, Office of Basic Energy Sciences, Office of Energy Research, U.S. Department of Energy under Contract No. DE-FG02-95ER14579 and by the National Science Foundation under Grant No. PHY99-87984.

[1] C. S. Wood *et al.*, Science **275**, 1759 (1997).
[2] T. Udem, J. Reichert, R. Holzwarth, and T. W. Hänsch, Phys. Rev. Lett. **82**, 3568 (1999).
[3] V. Gerginov, A. Derevianko, and C. E. Tanner, Phys. Rev. Lett. **91**, 072501 (2003).
[4] C. Amiot, O. Dulieu, R. F. Gutterres, and F. Masnou-Seeuws, Phys. Rev. A **66**, 052506 (2002).
[5] M. S. Safronova, W. R. Johnson, and A. Derevianko, Phys. Rev. A **60**, 4476 (1999).
[6] A. Peters, K. Y. Chung, and S. Chu, Nature (London) **400**, 849 (1999).
[7] A. Peters *et al.*, Philos. Trans. R. Soc. London, Ser. A **355**, 2233 (1997).
[8] T. Udem, J. Reichert, T. W. Hänsch, and M. Kourogi, Phys. Rev. A **62**, 031801 (2000).
[9] J. Ye, S. Swartz, P. Jungner, and J. L. Hall, Opt. Lett. **21**, 1280 (1996).
[10] J. Helmcke *et al.*, IEEE Trans. Instrum. Meas. **52**, 250 (2003).
[11] P. C. Pastor *et al.*, Phys. Rev. Lett. **92**, 023001 (2004).
[12] G. Ferrari *et al.*, Phys. Rev. Lett. **91**, 243002 (2003).
[13] T. M. Ramond, S. A. Diddams, L. Hollberg, and A. Bartels, Opt. Lett. **27**, 1842 (2002).
[14] S. A. Diddams *et al.*, Top. Quantum Electron. **9**, 1072 (2003).
[15] A. Bartels and H. Kurz, Opt. Lett. **27**, 1839 (2002).
[16] T. Udem *et al.*, Phys. Rev. Lett. **86**, 4996 (2001).
[17] D. J. Jones *et al.*, Science **288**, 635 (2000).
[18] S. R. Jefferts *et al.*, Metrologia **39**, 321 (2002).
[19] V. Gerginov and C. E. Tanner, Opt. Commun. **222**, 17 (2003).
[20] V. Gerginov and C. E. Tanner, Opt. Commun. **216**, 391 (2003).
[21] W. H. Press, S. A. Teukolsky, W. T. Vetterling, and B. P. Flannery, *Numerical Recipes in FORTRAN*, 2nd ed. (Cambridge University Press, New York, 1992).
[22] A. Peters, K. Y. Chung, and S. Chu, Metrologia **38**, 25 (2001).
[23] J. M. Hensley, A. Wicht, B. C. Young, and S. Chu, in *Atomic Physics 17*, edited by E. Arimondo, P. DeNatale, and M. Inguscio (AIP, New York, 2001).